ACS OMEGA

http://pubs.acs.org/journal/acsodf

Article

Prosopis juliflora Seed Waste as Biochar for the Removal of Blue Methylene: A Thermodynamic and Kinetic Study

Carlos Diaz-Uribe, Luis Walteros, Freider Duran, William Vallejo,* and Arnold R. Romero Bohórquez

Cite This: *ACS Omega* 2022, 7, 42916−42925

Read Online

ACCESS | Metrics & More | Article Recommendations | Supporting Information

ABSTRACT: In this work, we studied the methylene blue (MB) dye adsorption capacity on biochar derived from residues of *Prosopis juliflora* seed waste, a species found in the region of the tropical dry forest of Piojó in the Department of Atlántico, Colombia. The materials were obtained by pyrolysis at temperatures of 300, 500, and 700 °C. Biochar was characterized using Fourier transform infrared (FTIR), scanning electron microscopy and energy-dispersive X-ray spectroscopy (SEM-EDX), TGA, and Brunauer−Emmett−Teller (BET) techniques. The three biochar samples presented a macroporous, rough structure with pore size between 6 and 28 μm. The largest pore surface area observed was 1.28 m^2/g for pyrolyzed biochar produced at 500 °C, larger than that of biochar produced at 700 °C, which was 0.83 m^2/g. The adsorption results show that the maximum percentage of MB removal was 69%. According to SEM results, the material's pore sizes varied on average from 6 to 28 μm. We modeled MB adsorption on biomass through three different isotherm models. The Freundlich model was the best-fitting model for the removal of MB (K_F = 1.447; $1/n$ = 0.352). The kinetic results showed that the pseudo-second-order model was the best-fitting model for the sorption process (q_e = 2.94 mg/g; k_2 = 0.087 g/(mg/min^{-1})). Furthermore, the recycling test showed that the biochar did not change its adsorption capacity significantly. Finally, under the experimental conditions, the thermodynamic parameters indicated that the removal of MB using biochar was an endothermic and spontaneous process; all $\Delta G°$ values ranged from −2.14 to −0.95 kJ/mol; $\Delta H°$ was 23.54 kJ/mol and $\Delta S°$ was 79.5 J/mol.

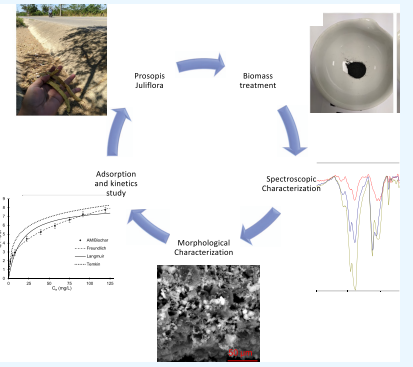

1. INTRODUCTION

Many water bodies are polluted by solid waste and chemical substances (organic and inorganic nature) that are harmful to the environment.[1,2] Most of these compounds come from industrial activity. These anthropogenic activities produce waste that runs through surface and groundwater and reaches water bodies through processes such as leaching and runoff.[3] Textile industries generate a diversity of pollutants; among these are dyes, which commonly result from textile-waste processes. Azo dyes are applied in dyeing processes due to their high activity; reports indicate that 50−70% of the total dye quantity employed in textile, plastic, and paper industries can involve these dyes.[4] Some of these compounds are hardly biodegradable, in addition to the fact that traditional treatments cannot break down recalcitrant dyes.[5,6] In an aquatic environment, these compounds can settle on the entire surface of the water body and adsorb much of the sunlight, preventing photosynthetic organisms from accessing the energy they need, therefore decreasing the productivity of photosynthetic species, the concentration of dissolved oxygen and, in turn, increasing both the chemical oxygen demand (COD) and the biochemical oxygen demand (BOD).[7,8] Furthermore, the production of toxic intermediates resulting from the decomposition of dyes by environmental factors affects the variability of species in flora and fauna.[9,10] Methylene blue (MB) is an organic cationic dye characterized by its intense bluish color, with applications in the textile, biological, chemical, and medical industries.[11] MB is a tricyclic phenothiazine, soluble in water.[12] MB dyes can generate intermediate substances, some of them highly toxic for their carcinogenic or mutagenic characteristics.[13] Currently, various techniques are applied to eliminate waste coming from food or textile industries, either through biological processes (e.g., bioremediation or biological filtration)[14] or phase change processes (e.g., sorption,[15,16] biological, advanced oxidation[17] and, sono-photocatalytic degradation[18,19]). Although advanced oxidation processes are very efficient in mineralizing dyes, their application is limited due to financial factors (e.g., higher costs both on chemicals and energy consumption).[20] Moreover, in some cases, a second process is necessary to remove residual oxidants or unknown recalcitrant byproducts.[21] Biological processes include (i) biological filtration, (ii) bioremediation, and (iii) the use of active sludge and activated sludge or mud.[22,23] However, these methods have some drawbacks, as

Received: August 5, 2022
Accepted: November 2, 2022
Published: November 14, 2022

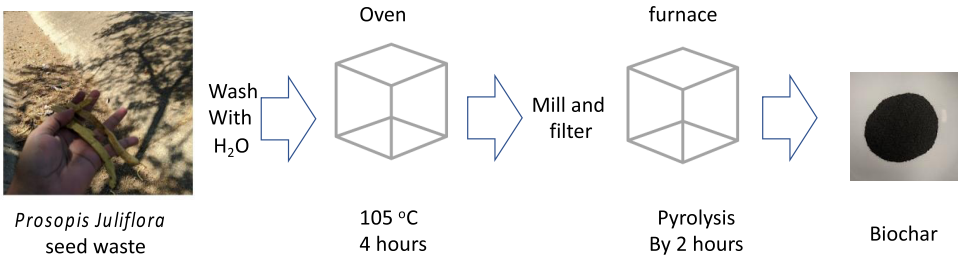

Figure 1. Schemcatic process of the biochar synthesis.

they (i) require a large surface area of land, (ii) demand a longer time for discoloration-fermentation processes, and (iii) are unable to remove dyes continuously.[24]

With the increase of emerging contaminants in wastewater, adsorption has become an effective and affordable mechanism to treat them. Adsorption is a phase change technology capable of transferring contaminants from one phase to another. This technology includes the following adsorption methods: adsorption by activated carbon, adsorption by biochar; adsorption by nanomaterials, adsorption by membranes, and adsorption by clay minerals.[25] Given their adsorption capacity, porous structure, and large surface area, activated carbons have proven to be an important alternative as an adsorption technology.[26] The main drawback thereof is the high cost of regeneration and the raw material necessary for their activation, given that activated carbons need chemical agents to improve their adsorption capacity.[27] Adsorption based on biomass sources (named biochar) can eliminate the contaminants from wastewater of textile industries, with the advantage of being both more economical and more ecological than commercial adsorbents.[28] Different biomass sources have been reported to remove methylene blue from water bodies (e.g., corn cob residues,[29] rice husk,[30] mango leaves,[31] microalgae[32]). Currently, the use of biomass as a potential adsorbent is an important goal to be achieved in the scope of adsorption technologies.[33]

Agricultural waste is misled or discarded in most countries due to either unawareness or a proper channel to transfer and utilize it.[34] Agricultural and other natural waste components have the potential to become biochar, and in the Caribbean region there is a variety of natural waste available to be used as biochar. The *Prosopis juliflora* plant species can be found in the tropical dry forest region of Piojó and other municipalities of the Department of Atlántico, Colombia.[35] This plant is used to reduce the internal temperature of houses in the region. During the first quarter of the year, the species begins to produce its seeds, which become waste that is later burned or discarded as solid waste. Furthermore, the *P. juliflora* plant contributes to enhancing the transmission capacity of malaria disease.[36] In this work, we produced biochar from *P. juliflora* waste seeds obtained from the houses of residents of Piojó. We studied the effect of pyrolysis temperature on the physicochemical properties of biochar. We investigated the adsorption capacity of methylene blue on biochar, in addition to analyzing the adsorption mechanism of this dye by means of adsorption isotherm and kinetic studies. Finally, we carried out a thermodynamic study of the process.

2. EXPERIMENTAL SECTION

2.1. Biomass Source Location and Biochar Synthesis. Biomass samples were collected from houses and farms in the district of Hibácharo, municipality of Piojó, Department of Atlántico, Colombia (GPS coordinates 10°45′01″ N 75°06′27″ O) [see the Supporting Information for further details, Figures S1 and S2]. The collected *P. juliflora* waste seeds were washed with potable water to clean their outer surface and were later dried in an oven at 105 °C for 4 h. Finally, the clean seeds were milled and then proceeded to the synthesis process.[37,38] The resulting biomass was put in a pyrolysis reactor (Terrigeno-brand) in a nitrogen atmosphere (500 mLN_2/min) for 30 min. Pyrolysis was then performed at a heating rate of 5 °C/min^{-1} at three different temperatures (300 °C (biochar 1), 500 °C (biochar 2), and 700 °C (biochar 3)). The pyrolysis process started at ambient temperature and the exposition time at each temperature was 2 h; Figure 1 shows a scheme of the biochar fabrication.[39,40]

2.2. Biochar Characterization. The physical−chemical properties of biochar were examined through (i) Fourier transform infrared (FTIR)-spectroscopy (using an ECO-ATR α Bruker FTIR spectrometer); (ii) thermogravimetric analysis (using a TA Instruments TGA 5500-Discovery analyzer), with an N_2 flow of 25 cm^3/min and a heating rate of 5−20 °C/min from 25 until 800 °C; (iii) the Brunauer−Emmett−Teller (BET) method, with N_2 physisorption at 77 K (using a Micromeritics 3Flex N_2 sortometer); and (iv) scanning electron microscopy and energy-dispersive X-ray spectroscopy (SEM-EDX) (using an FEI Quanta FEG 650 microscope). For the chemical assay, we used an EDAX Apollo X detector (126.1 eV resolution) and EDX Genesis software.

2.3. Adsorption Isotherm Study. Due to its low cost and risk, methylene blue (MB) is considered a model molecule for the study of mechanisms of adsorption of cationic dyes by new biochars.[41] The effect of MB concentration on adsorption was studied between the range 10 and 150 mg/L (initial concentration of MB = 10, 15, 20, 40, 60, 80, 100, 120, and 150 mg/L). The volume of the solution was 25 mL, pH 6.0, and a biochar load was 0.100. In each assay, the samples were kept in constant agitation for 3 h at 150 rpm and a temperature of 298 K. The concentration of MB was determined by UV−vis spectrophotometry at 665 nm (using a Shimadzu UV-2401PC UV−vis spectrophotometer). The adsorption capacity of MB on the biochar surface was determined using the following equation

$$q_e = \frac{V(C_0 - C_e)}{m} \quad (1)$$

where q_e is the amount (mg) of MB adsorbed per gram of biochar (mg/g) at equilibrium, C_0 is the initial MB concentration (mg/L), C_e is the MB concentration at equilibrium, V (L) is the volume of the system, and m (g) is the amount of biochar. Adsorption data were fitted to the Freundlich, Langmuir, and Temkin isotherm models.[42] Table 1

https://doi.org/10.1021/acsomega.2c05007
ACS Omega 2022, 7, 42916−42925

Table 1. List of Equations for Isotherm and Kinetic Fitting[42,43]

model	equation	parameters
Langmuir equation	$q_e = \frac{q_m K_L C_e}{1 + K_L C_e}$	q_e(mg/g) is the MB amount (mg) adsorbed on biomass (g) at equilibrium condition; q_m is the Langmuir maximum uptake of MB per gram of biomass (mg/g); and K_L(L/mg) is the Langmuir constant.
Freundlich equation	$q_e = K_F C_e^{1/n}$	K_F((mg/g) (L/mg)1/n) and n are Freundlich constants and C_e(mg/L) is the equilibrium concentration of MB.
Temkin isotherm	$q_e BLn(A_T C_e)$	B is the Temkin constant associated with the parameter b_T by the relation $b_T = \frac{RT}{B}$, A_T is the equilibrium binding constant (L/mg), T is the absolute temperature, and R is the gas constant.
pseudo-first order	$\ln(q_t - q_e) = \ln(q_e) - k_1 t$	q_t is the MB amount (g) adsorbed by gram of the biochar surface at time t (min), q_e is the same ratio at the equilibrium, k_1(min^{-1}) and k_2(g/mg·min) are the rate constants of the pseudo-first and pseudo-second-order models, respectively. The k_{id}(mg/g·min$^{1/2}$) is the intraparticle diffusion rate constant.
pseudo-second order	$\frac{t}{q_t} = \frac{1}{k_2 q_e^2} + \frac{t}{q_e}$	
Intraparticle diffusion	$q_t = k_{id} t^{1/2} + C$	

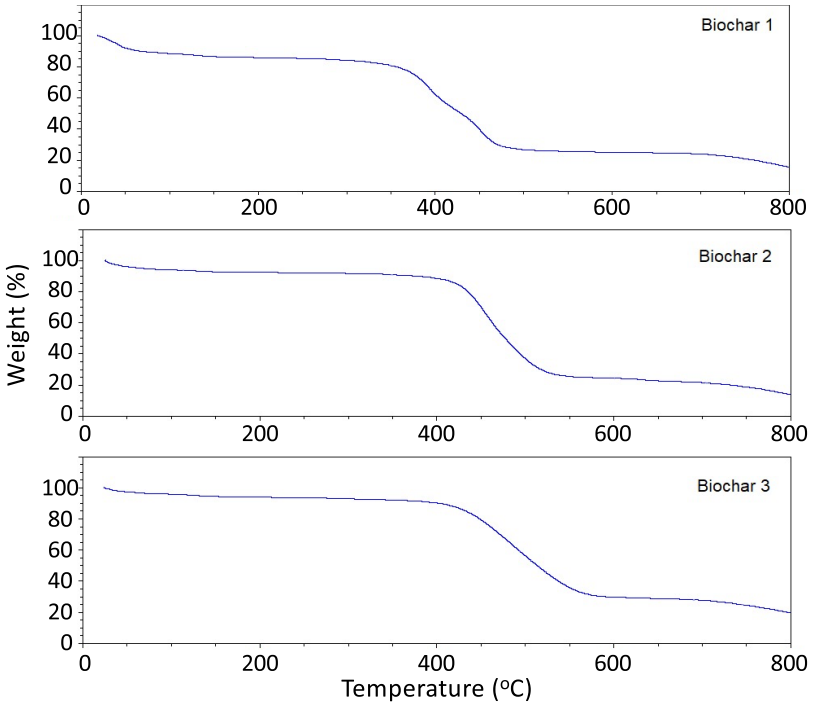

Figure 2. TGA for biochars obtained from *P. juliflora* by pyrolysis at 300 °C (biochar 1), 500 °C (biochar 2), and 700 °C (biochar 3).

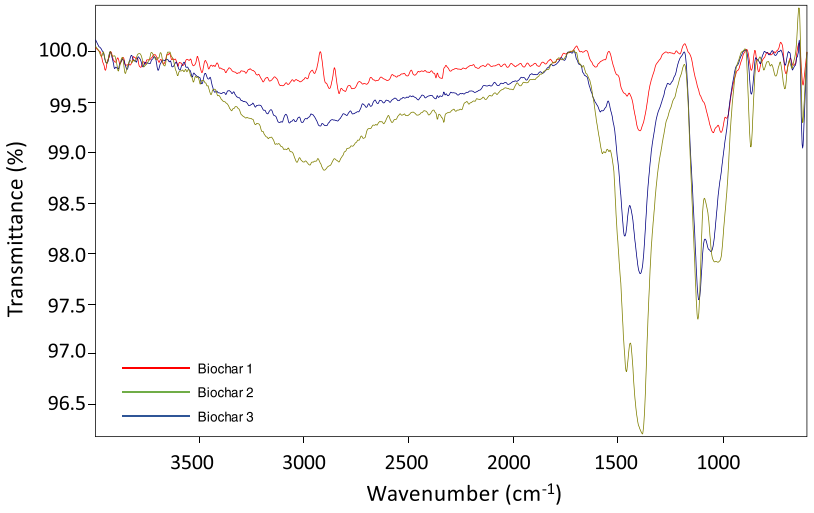

Figure 3. FTIR spectra of biochars obtained from *P. juliflora* by pyrolysis at 300 °C (biochar 1), 500 °C (biochar 2), and 700 °C (biochar 3).

lists the equations and corresponding physical−chemical parameters.[43] A fitting correlation coefficient (R^2) and an average relative error (ARE) were used to determine the best-fitting isotherm

https://doi.org/10.1021/acsomega.2c05007
ACS Omega 2022, 7, 42916−42925

$$\mathrm{ARE} = \frac{100}{n}\sum_{i=1}^{n}\frac{|q_e - q_f|}{q_e} \quad (2)$$

where q_e is the experimental value, q_f is the fitted value, and n is the number of data points. Details of fitting parameters are given in Table 1.

2.5. Adsorption Kinetics and Thermodynamic Study. We determined the amount of MB adsorbed onto biochar as a function of time according to the following equation

$$q_t = \frac{((C_0 - C_t)\cdot V)}{m} \quad (3)$$

where C_t (mg/L) is the concentration of MB in the solution at time t (min). We employed three adsorption kinetic models to fit the experimental data: (a) pseudo-first-order, (b) pseudo-second-order, and (c) intraparticle diffusion.[44] The thermodynamic parameters of the adsorption process, Gibbs free energy ($\Delta G°$), enthalpy ($\Delta H°$), and entropy ($\Delta S°$) were determined according to[45]

$$K = \frac{q_e}{C_e} \quad (4)$$

$$\Delta G° = -RT \ln K \quad (5)$$

$$\ln K = \frac{\Delta S°}{T} - \frac{\Delta H°}{RT} \quad (6)$$

where T is the absolute temperature (K), R is the universal gas constant (8.314 J/mol·K), and K is the thermodynamic equilibrium constant.

3. RESULTS AND DISCUSSION

3.1. Biochar Yield. After the pyrolysis process, the biochar yield is affected by the experimental conditions, such as temperature and residence time, along with the type and properties of the raw material (e.g., water content, cellulose, hemicellulose, lignin). Lignin is more stable than cellulose and hemicellulose and contributes significantly to biochar yield.[46] *P. juliflora* has a typical content of 40−44% cellulose, 25−30% hemicellulose, and 20−22% lignin.[47] We studied the effect of temperature on biochar yield. The highest biochar yield percentage (34.12%) was obtained at 300 °C, then decreased to 19.45% at 500 °C, and finally 17.22% at 700 °C. These changes are associated with different aspects: cellulosic degradation and depolymerization, dehydration, volatilization, and concentration of aliphatic and aromatic carbon-containing systems.[48] Because of its high content of cellulose and hemicellulose, biomass can degrade at low temperatures (between 200 and 400 °C).[49] At higher pyrolysis temperatures, biomass carbonization through rapid dehydrogenation, gasification, and condensation increases, resulting in a marked reduction in solid biochar yield.

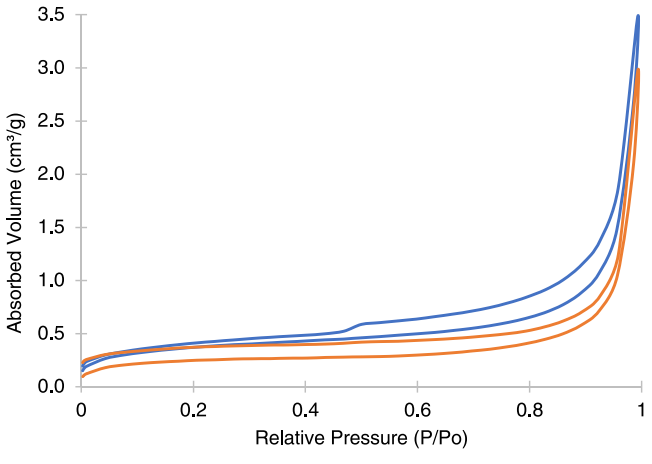

Figure 4. N_2 physisorption isotherms of biochar 2 (blue line) and biochar 3 (red line).

3.2. Biochar Characterization. *3.2.1. Thermogravimetric Assay.* Figure 2 shows thermogravimetric curves for the three different temperatures analyzed. Temperatures between 25 and 45 °C presented slight weight losses of approximately 5% for biochars 2 and 3 and close to 11% for biochar 1, possibly due to the loss of water and volatilization of low-molecular-weight organic solvents.[50] Figure 2 shows a weight loss of 68% for biochars 2 and 3 between temperatures 420 and 570 °C and 60% for biochar 1 between temperatures 370 and 470 °C. These results are associated with the thermic degradation of cellulose and oxidation of lignin.[51] Finally, Figure 2 shows a weight of approximately 10% between temperatures 470 and 800 °C for biochar 1 and between 570 and 800 °C for biochars 2 and 3. This behavior is associated with carbonization and thermochemical transformation (e.g., demethylation and decarboxylation reactions).[52]

Through pyrolysis, the basic organic components of raw materials, such as hemicellulose, cellulose, and lignin, degraded between 200 and 600 °C. Depending on the pyrolysis temperature, different structural compositions of cellulose, hemicellulose, and lignin lead to thermal decomposition differences and, therefore, to different remaining percentages of these compounds in the final biochar.[53] After cellulose degradation, the lignin content continues to decompose from 400 to 800 °C; this is the most complex polymer of lignocellulosic biomass and requires high temperatures and more time for decomposition. Unlike hemicellulose and cellulose, lignin is composed of stable benzene−propane units of high molecular weight, hence difficult to be broken down. Lignin derivatives are responsible for the generation of phenolic products.[54] Figure S3 shows a general scheme of pathway reaction of the pyrolysis process.[55]

3.2.2. FTIR Assay. Figure 3 shows the FTIR spectra of the biochars obtained from *P. juliflora* by pyrolysis at three different temperatures. The band located between 3200 and 2800 cm^{-1} is assigned to asymmetrical and symmetrical stretch vibrations of the C−H bond (e.g., methyl and methylene groups); these groups appear as a result of tarry remains that partially volatilized, but these could be present in the initial structure of biochar.[56,57] The bands located between 1600 and 1400 cm^{-1} are assigned to carbon−carbon stretching vibrations in the aromatic ring, alkene groups.[58] The bands located between 1200 and 1000 cm^{-1} are assigned to the stretching vibration of the C−O bond (e.g., carboxylic acids in the cellulose and hemicellulose).[59] Finally, the bands located between 800 and 700 cm^{-1} are assigned to the bending vibration of the C−H bond.

In the pyrolysis process, temperature affects the final functional groups present on the biochar surface. As the pyrolysis temperature increases from 300 to 500 °C, the number of intense bands increases, and this is due to the process of aromatization and degradation of lignocellulosic components, such as dehydrogenation reactions.[57] The intensity of the signals reducing at 700 °C is associated with

https://doi.org/10.1021/acsomega.2c05007
ACS Omega 2022, 7, 42916−42925

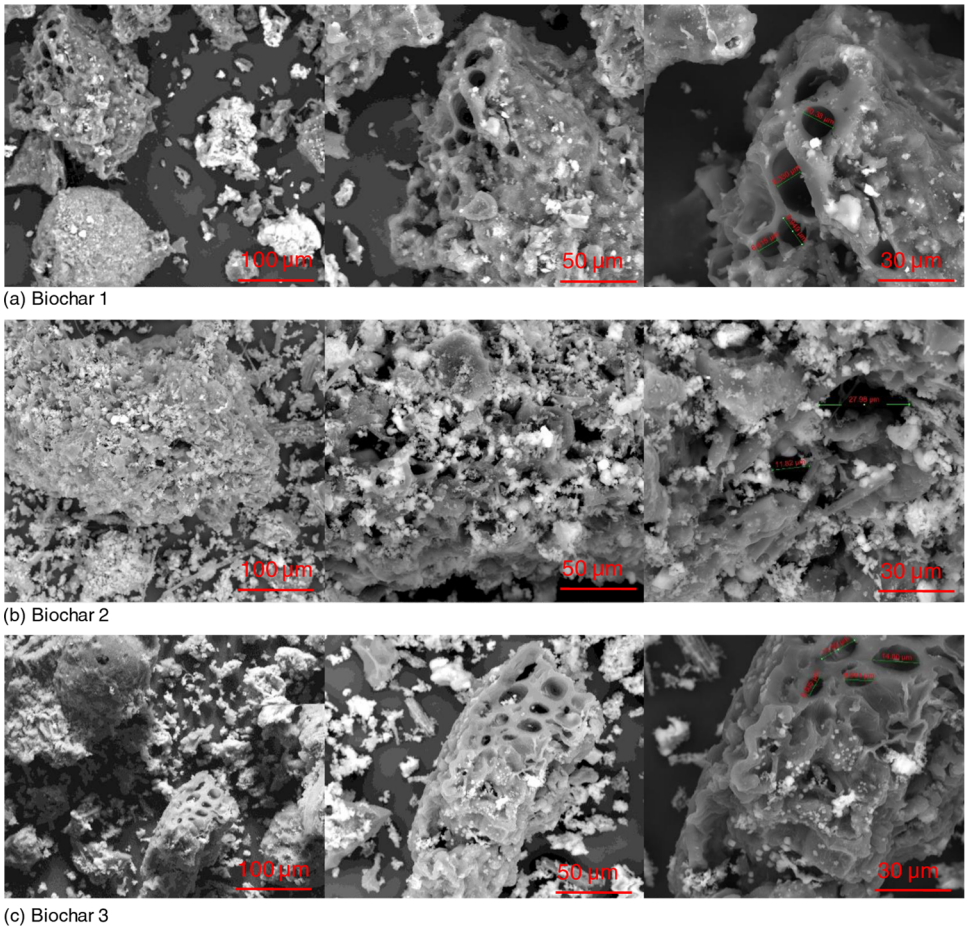

Figure 5. SEM images of *P. juliflora* obtained by pyrolysis at (a) 300 °C (biochar 1), (b) 500 °C (biochar 2), and (c) 700 °C (biochar 3).

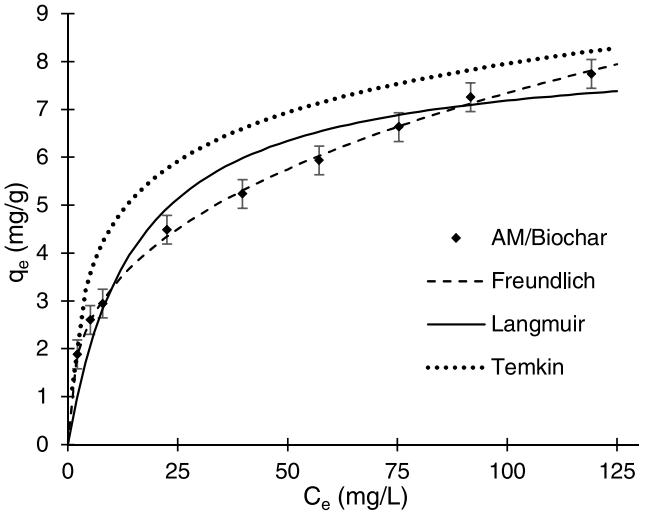

Figure 6. Fitting adsorption isotherm models for MB adsorption onto biochar 2.

the biomass degradation process (e.g., dehydration and deoxygenation reactions), which leads to reducing the content of polar functional groups and other functional groups containing hydrogen and oxygen, thus suggesting that aliphatic compounds can be highly aromatized during the carbonization process.[60]

3.2.3. BET Assay. Figure 4 shows the BET nitrogen isotherms of the sampled biochar (2 and 3). According to

Table 2. Isotherm Model Parameters

isotherm model	parameters			
Langmuir	q_{max}(mg/g)	K_L(L/mg)	R^2	ARE (%)
	8.285	0.0651	0.981	12.9
Freundlich	K_F(mg/g)(L/mg)$^{1/n}$	$1/n$	R^2	ARE (%)
	1.4469	0.352	0.999	0.03
Temkin	A (L/mg)	K_T (L/g)	R^2	ARE (%)
	1.47	1.17	0.918	8.0

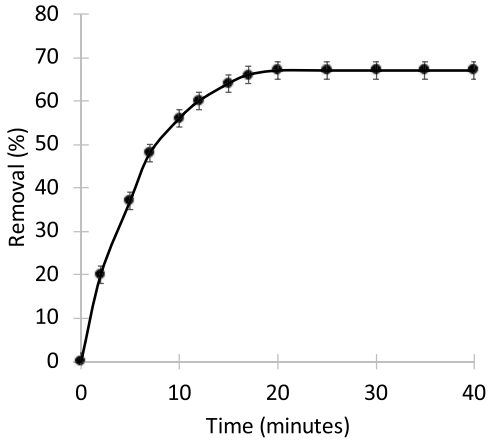

Figure 7. MB adsorption as a function of contact time on biochar 2.

https://doi.org/10.1021/acsomega.2c05007
ACS Omega 2022, 7, 42916−42925

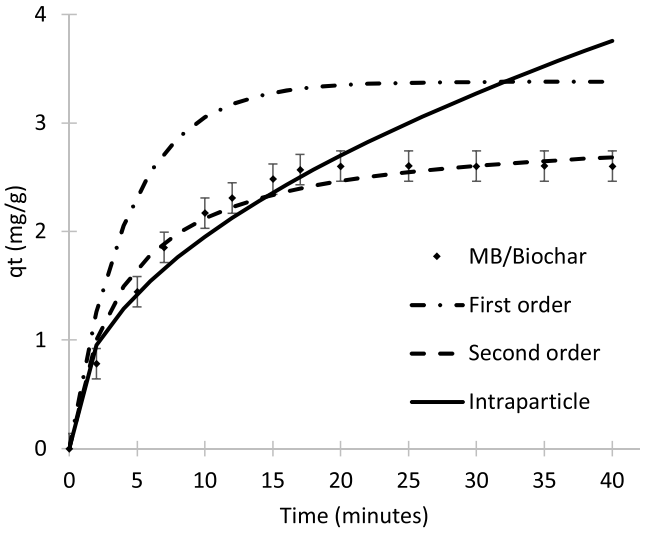

Figure 8. Adsorption kinetics for MB onto biochar 2.

Table 3. Kinetic Values Calculated for MB Sorption onto Biochar 2

model	parameters			
pseudo-first order	q_e (mg/g)	k_1 (min^{-1})	R^2	ARE (%)
	3.38	0.234	0.947	38.1
pseudo-second order	q_e(mg/g)	k_2(g/(mg·min))	R^2	ARE (%)
	2.94	0.087	0.992	8.4
intraparticle diffusion	C(mg/g)	k_{id}(g/(mg·min))	R^2	ARE (%)
	0.147	0.571	0.949	11.9

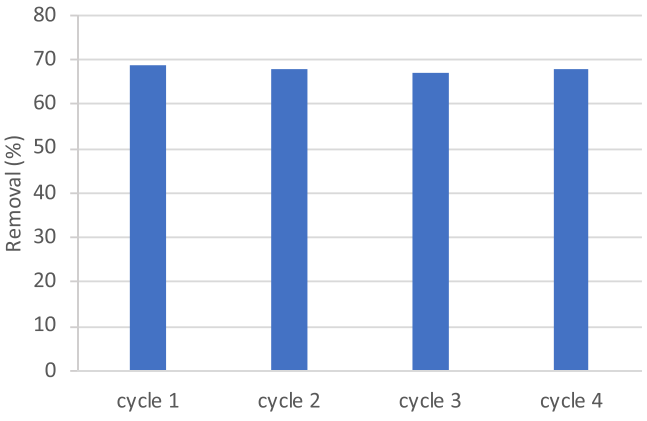

Figure 9. Recycling test for adsorption capacity of MB onto biochar 2.

the IUPAC nomenclature,[61] biochar isotherms are type II, with H3-type hysteresis. This behavior is associated with solids constituted of laminar packages or solids constituted of pores with a crack-like shape (e.g., activated carbons).[62] The BET surface area of biochar 2 was 1.28 m^2/g, and of biochar 3, it was 0.83 m^2/g (the reduced surface area of biochar 1 did not allow obtaining the BET nitrogen isotherms). As observed, the surface area increased with increasing pyrolysis temperature. This phenomenon can be attributed to the evaporation and gradual decomposition of volatile organic components as the pyrolysis temperature increases, making the carbon matrix structure highly concentrated, generating more pores in the structure and favoring the development of a larger surface area.[63] The biochars obtained from straw, seeds, or fruit shells show less developed structures than those with abundant lignin; therefore, the former produce more ash and have smaller surfaces, compared to biochars produced with other types of biomasses. The low surface area of biochar 3 can be attributed to a high ash content present on the surface, blocking either the meso-, micro-, or macropores.[64]

Another study reported that the surface area of biochar increases with increasing temperatures below 600 °C but decreases at temperatures above 700 °C.[65] Besides, biochars produced from cotton stalks slightly increased their surface area with increasing pyrolysis temperature; however, this area decreased when the temperature increased to 650 °C due to pores collapsing and channels becoming blocked at high temperatures.[66] The type of isotherm and the surface area are characteristic of macroporous solids with a diameter of approximately 50 nm, a result that could be ratified by SEM analysis. Our results are according to other reports; Pawar et al. reported a BET surface area value of 0987 m^2/g to biochar derived from *P. juliflora*.[67]

3.2.4. SEM-EDX Assay. The changes in surface morphology and elemental components on the surface of the three biochar samples obtained were studied by SEM-EDX analysis. Figure 5 shows the SEM micrographs of the samples. The surface morphology of all biochars was heterogeneous, structurally complex, and with additional porosity forming during thermal conversion. The images clearly show macroporous and rough surface textures. The obtained biochars showed a surface with an incomplete pore structure, which is consistent with their low value of the surface area. Porosity is a consequence of the release of matter in the form of small volatile molecules (H_2O, CO, CO_2, and CH_4) during the thermal conversion process.[68] When the temperature increases, the surface of the biochar becomes rougher, and more pore structures appear. Due to the persistence of organic matter in the biochar network at low temperatures (300 °C), the pores did not develop totally. In biochar 2, changes in microscopic morphology were observed as the pores were revealed. The underlying pores widened due to the removal of volatile matter.[69] At higher temperatures (e.g., 700 °C), carbon deposition and sintering of inorganic compounds may occur. Figure 5c shows the collapse of the pore structure, which attributes a lower value of the surface area to biochar 2. This can be explained because lignin pyrolysis produces tars (condensed volatiles) and other decomposition products that, in turn, partially block the pores of the biochar surface.[70] In some areas, the biochar samples contain a large part of arranged structures, mostly of macroporous texture, in the form of a honeycomb. Pore sizes varied on average from 6 to 28 μm; but in some cases, these pores fused after pyrolysis to produce larger cavities.

According to the results of the EDX assay (Figure S4), all of the biochar samples analyzed consist mainly of carbon and oxygen; and the remaining elements are (i) nonmetallic (P and Cl) and (ii) metallic (K, Ca, Na and Mg). It is noted that the carbon content increases with increasing pyrolysis temperature while the oxygen content decreases. Heat treatment results in the gradual decomposition of organic macromolecules into raw materials, such as cellulose, hemicellulose, and lignin, which through dehydration and decarboxylation reactions of degradable and volatile carbon compounds, contribute to decreasing the hydrogen and oxygen contents.[71] Furthermore, the reactivity of coal gasification also depends on factors such as the presence of inorganic components. For example, potassium is known to impede the gasification process, and this may be a reason for the low surface area of the samples.

https://doi.org/10.1021/acsomega.2c05007
ACS Omega 2022, 7, 42916−42925

Table 4. Thermodynamic Parameters for Removal of MB from Different Types of Carbon-Based Adsorbents

carbon-source adsorbent	isotherm model	temperature (K)	thermodynamic parameters		
			ΔG(kJ/mol)	ΔH(kJ/mol)	ΔS(J/mol)
biochar 2/this work	Freundlich	308	−0.95	23.54	79.5
		313	−1.34		
		318	−1.74		
		323	−2.14		
Acacia fumosa seed[83]	Langmuir	303	−0.29	3.66	61.55
		313	−0.23		
		323	−0.17		
sucrose spherical carbon[80]	Redliche−Peterson	298	−1.71	16.3	0.060
		308	−1.91		
		318	−2.91		
Pongamia pinnata fruit hulls[84]	Langmuir	303	−0.269	38.88	130
		313	−2.062		
		323	−2.841		
chemically modified lychee seed biochar[85]	Langmuir	303	−9.65	18.98	94.5
		313	−10.59		
		323	−11.54		
Morus nigra L. leaves[86]	Langmuir	283	−0.87	−13.92	−30
		293	−1.19		
		303	−1.36		

Previous research has shown that the presence of inorganic components such as K, Na, Ca, Fe, and Mg affects the overall reactivity of gasification.[72]

3.3. Adsorption Isotherms. Due to its higher surface area, we choose biochar 2 to perform the sorption study. Models of adsorption isotherms can be used to examine the interaction between methylene blue dye and biochar. We used three different models of isotherms: Langmuir, Freundlich, and Temkin, which are the most used for this type of adsorbent.[73]Figure 6 shows the experimental isotherm and the fitting to the models proposed, and Table 2 lists the adsorption isotherm parameters.

According to Figure 6 and Table 2, the Freundlich adsorption isotherm is the best-fitting model for the experimental results. The adsorption of the dye onto biochar is characterized as a multilayer and with a heterogeneous surface. This result agrees with the morphology exhibited by the spectroscopic and SEM assay. The presence of different functional groups (e.g., aromatic rings, −C═O, −C−O−C−, −OH) on the biochar surface has a special role in increasing the adsorption capacity of methylene blue.[74] The value of $1/n$ = 0.352 indicates that the adsorption process is favorable.[75]

3.4. Adsorption Kinetics. The effect of contact time is shown in Figure 7. It can be observed that the percentage of removal of methylene blue increases with increasing contact time, indicating the greater availability of active sites on the biochar surface up to saturation after 17 min. At the initial stage of the adsorption process on the biochar surface, there are many negatively charged active sites available, then sorption occurs rapidly and is normally controlled by the diffusion process from volume to surface at the beginning of adsorption. At the later stage, sorption is likely to be a controlled process due to the lower availability of active sites. The kinetic mechanism of methylene blue adsorption onto biochar can be studied indirectly using different kinetic models. In this work, three different models were used. Figure 8 shows the adjustment of the adsorption kinetic models, and Table 3 shows the parameters obtained. The pseudo-second-order model showed the best-fitting regression values (higher R^2 and lower ARE values). These results suggest that chemisorption is the dominant interaction during the adsorption of methylene blue onto the biochar surface, where effective electrostatic interactions play an important role in adsorption, and a chemical reaction (e.g., complexation, ion exchange, precipitation) could be present during the adsorption process.[76] Finally, the pseudo-second-order model is commonly reported as the best-fit model in the adsorption studies of different pollutants on biochar.[77,78]

The stability of the adsorbents is an important parameter in developing practical applications. Figure 9 shows the results of the adsorption of MB after four cycles on the same biochar sample. After the 4th cycle, the adsorption capacity decreases by 1.0%. The percentage reduction was not significant, suggesting that the biochar was stable to a constant adsorption/desorption process after four cycles.

3.5. Adsorption Thermodynamic Study. We studied the MB adsorption process onto biochar 2 at different temperatures (308, 313, 318, and 323 K). The thermodynamic parameters $\Delta H°$ and $\Delta S°$ were calculated from the slope and intercept of the linear fitting of the Arrhenius equation ln K vs $1/T$ (see eq 6). Table 3 lists the thermodynamic parameters of the BM adsorption process on biochar 2 and other different types of carbon-based adsorbents.[79] The negative $\Delta G°$ values indicate that the removal of MB using biochar 2 is a spontaneous process. The reduction of $\Delta G°$ at higher temperatures shows the viability of adsorption at higher temperatures. The $\Delta H°$ value indicates that the process is endothermic. The endothermic type of adsorption is also an indication of chemical adsorption. Positive adsorption entropy may be interrelated with the degree of hydration of cationic dye molecules. This result suggests an increase in randomness at the adsorbent−liquid interface during MB adsorption, with possible structural changes or interactions between MB molecules and the biochar.[80−82] Kumar et al. suggest that the positive change in the entropy value implies that the conscious choice of an adsorbent increases with the increase of an orderliness between the adsorbate and the adsorbent molecules.[83] Results obtained to biochar 2 with other reports

https://doi.org/10.1021/acsomega.2c05007
ACS Omega 2022, 7, 42916−42925

for removal of MB on different types of carbon-based adsorbents (Table 4) are comparable, the value of free energy in all cases is negative, and the values of ΔH and ΔS are comparable. Our results indicate that the biochar produced from natural waste is a suitable option for the removal of MB from aqueous samples.

4. CONCLUSIONS

In this work, new biochar was produced from *P. juliflora* waste seeds. It was used as an alternative adsorbent to remove methylene blue from the aqueous samples. The thermogravimetric analysis showed that the biochar produced between 500 and 700 °C had greater stability than the biochar produced at 300 °C. The three biochar samples presented a macroporous and rough structure. The biochars produced at temperatures between 500 and 700 °C presented isotherm type II with H3-type hysteresis. Studies of isotherms showed that the Freundlich model is the best-fitting model for the removal of methylene blue. The kinetic results showed that the pseudo-second-order model was the best-fitting model for the sorption process. Under experimental conditions, the thermodynamic parameters indicated that the removal of MB using biochar 2 was endothermic and a spontaneous process. Finally, results indicated that *P. juliflora* seed waste is an alternative source to obtaining biochar with adsorption capacity of MB.

■ ASSOCIATED CONTENT

Supporting Information

The Supporting Information is available free of charge at https://pubs.acs.org/doi/10.1021/acsomega.2c05007.

(Figure S1) Location of the biomass collection place, (Figure S2) *P. juliflora* waste seeds, (Figure S3) general scheme of the pathway reaction of the pyrolysis process, and (Figure S4) EDX spectrum of *P. juliflora* (PDF)

■ AUTHOR INFORMATION

Corresponding Author

William Vallejo − *Grupo de Investigación en Fotoquímica y Fotobiología, Programa de Química, Facultad de Ciencias Básicas, Universidad del Atlántico, Puerto Colombia 081007, Colombia*; orcid.org/0000-0002-6661-545X; Email: williamvallejo@mail.uniatlantico.edu.co

Authors

Carlos Diaz-Uribe − *Grupo de Investigación en Fotoquímica y Fotobiología, Programa de Química, Facultad de Ciencias Básicas, Universidad del Atlántico, Puerto Colombia 081007, Colombia*

Luis Walteros − *Grupo de Investigación en Fotoquímica y Fotobiología, Programa de Química, Facultad de Ciencias Básicas, Universidad del Atlántico, Puerto Colombia 081007, Colombia*

Freider Duran − *Grupo de Investigación en Fotoquímica y Fotobiología, Programa de Química, Facultad de Ciencias Básicas, Universidad del Atlántico, Puerto Colombia 081007, Colombia*

Arnold R. Romero Bohórquez − *Grupo de Investigación en Compuestos Orgánicos de Interés Medicinal (CODEIM), Parque Tecnológico Guatiguará, Universidad Industrial de Santander, Bucaramanga 680002, Colombia*

Complete contact information is available at: https://pubs.acs.org/10.1021/acsomega.2c05007

Notes

The authors declare no competing financial interest.

■ ACKNOWLEDGMENTS

The authors thank Universidad del Atlántico and Universidad Industrial de Santander.

■ REFERENCES

(1) Madikizela, L. M. Removal of Organic Pollutants in Water Using Water Hyacinth (Eichhornia Crassipes). *J. Environ. Manage.* **2021**, *295*, No. 113153.

(2) Srivastav, A. L.; Ranjan, M. Inorganic Water Pollutants. *Inorg. Pollut. Water* **2020**, 1−15.

(3) Sullivan, G. L.; Delgado-Gallardo, J.; Watson, T. M.; Sarp, S. An Investigation into the Leaching of Micro and Nano Particles and Chemical Pollutants from Disposable Face Masks - Linked to the COVID-19 Pandemic. *Water Res.* **2021**, *196*, No. 117033.

(4) Al-Musawi, T. J.; Mengelizadeh, N.; Al Rawi, O.; Balarak, D. Capacity and Modeling of Acid Blue 113 Dye Adsorption onto Chitosan Magnetized by Fe2O3 Nanoparticles. *J. Polym. Environ.* **2021**, *30*, 344−359.

(5) Talaiekhozani, A.; Reza Mosayebi, M.; Fulazzaky, M. A.; Eskandari, Z.; Sanayee, R. Combination of TiO2 Microreactor and Electroflotation for Organic Pollutant Removal from Textile Dyeing Industry Wastewater. *Alexandria Eng. J.* **2020**, *59*, 549−563.

(6) Russo, A. V.; Merlo, B. G.; Jacobo, S. E. Adsorption and Catalytic Degradation of Tartrazine in Aqueous Medium by a Fe-Modified Zeolite. *Cleaner Eng. Technol.* **2021**, *4*, No. 100211.

(7) Lellis, B.; Fávaro-Polonio, C. Z.; Pamphile, J. A.; Polonio, J. C. Effects of Textile Dyes on Health and the Environment and Bioremediation Potential of Living Organisms. *Biotechnol. Res. Innovation* **2019**, *3*, 275−290.

(8) Sela, S. K.; Hossain, A. K. M. N. U.; Hussain, S. Z.; Hasan, N. Utilization of Prawn to Reduce the Value of BOD and COD of Textile Wastewater. *Cleaner Eng. Technol.* **2020**, *1*, No. 100021.

(9) El-Rahim, W. M. A.; Moawad, H.; Azeiz, A. Z. A.; Sadowsky, M. J. Biodegradation of Azo Dyes by Bacterial or Fungal Consortium and Identification of the Biodegradation Products. *Egypt. J. Aquat. Res.* **2021**, *47*, 269−276.

(10) Berradi, M.; Hsissou, R.; Khudhair, M.; Assouag, M.; Cherkaoui, O.; El Bachiri, A.; El Harfi, A. Textile Finishing Dyes and Their Impact on Aquatic Environs. *Heliyon* **2019**, *5*, No. e02711.

(11) Can-Terzi, B.; Goren, A. Y.; Okten, H. E.; Sofuoglu, S. C. Biosorption of Methylene Blue from Water by Live Lemna Minor. *Environ. Technol. Innovation* **2021**, *22*, No. 101432.

(12) Dabholkar, N.; Gorantla, S.; Dubey, S. K.; Alexander, A.; Taliyan, R.; Singhvi, G. Repurposing Methylene Blue in the Management of COVID-19: Mechanistic Aspects and Clinical Investigations. *Biomed. Pharmacother.* **2021**, *142*, No. 112023.

(13) Sakthisharmila, P.; Palanisamy, P. N.; Manikandan, P. Removal of Benzidine Based Textile Dye Using Different Metal Hydroxides Generated in Situ Electrochemical Treatment-A Comparative Study. *J. Cleaner Prod.* **2018**, *172*, 2206−2215.

(14) Ihsanullah, I.; Jamal, A.; Ilyas, M.; Zubair, M.; Khan, G.; Atieh, M. A. Bioremediation of Dyes: Current Status and Prospects. *J. Water Process Eng.* **2020**, *38*, No. 101680.

(15) Aigbe, U. O.; Osibote, O. A. Carbon Derived Nanomaterials for the Sorption of Heavy Metals from Aqueous Solution: A Review. *Environ. Nanotechnol., Monit. Manage.* **2021**, *16*, No. 100578.

(16) Balarak, D.; Zafariyan, M.; Igwegbe, C. A.; Onyechi, K. K.; Ighalo, J. O. Adsorption of Acid Blue 92 Dye from Aqueous Solutions by Single-Walled Carbon Nanotubes: Isothermal, Kinetic, and Thermodynamic Studies. *Environ. Process.* **2021**, *8*, 869−888.

(17) Kumar, V.; Shah, M. P. Advanced Oxidation Processes for Complex Wastewater Treatment. *Adv. Oxid. Processes Effluent Treat. Plants* **2021**, 1−31.

(18) Al-Musawi, T. J.; McKay, G.; Rajiv, P.; Mengelizadeh, N.; Balarak, D. Efficient Sonophotocatalytic Degradation of Acid Blue 113

Dye Using a Hybrid Nanocomposite of CoFe2O4 Nanoparticles Loaded on Multi-Walled Carbon Nanotubes. *J. Photochem. Photobiol., A* **2022**, *424*, No. 113617.
(19) Al-Musawi, T. J.; Mengelizadeh, N.; Taghavi, M.; Shehu, Z.; Balarak, D. Capability of Copper−Nickel Ferrite Nanoparticles Loaded onto Multi-Walled Carbon Nanotubes to Degrade Acid Blue 113 Dye in the Sonophotocatalytic Treatment Process. *Environ. Sci. Pollut. Res.* **2022**, *29*, 51703−51716.
(20) Joshi, S. M.; Gogate, P. R. Treatment of Landfill Leachate Using Different Configurations of Ultrasonic Reactors Combined with Advanced Oxidation Processes. *Sep. Purif. Technol.* **2019**, *211*, 10−18.
(21) Johnson, I.; Ali, M. A. S.; Kumar, M. Cyanobacteria/Microalgae for Distillery Wastewater Treatment- Past, Present and the Future. *Microb. Wastewater Treat.* **2019**, 195−236.
(22) Liu, H.; Zhang, J.; Lu, M.; Liang, L.; Zhang, H.; Wei, J. Biosynthesis Based Membrane Filtration Coupled with Iron Nanoparticles Reduction Process in Removal of Dyes. *Chem. Eng. J.* **2020**, *387*, No. 124202.
(23) Haddad, M.; Abid, S.; Hamdi, M.; Bouallagui, H. Reduction of Adsorbed Dyes Content in the Discharged Sludge Coming from an Industrial Textile Wastewater Treatment Plant Using Aerobic Activated Sludge Process. *J. Environ. Manage.* **2018**, *223*, 936−946.
(24) Machineni, L. Review on Biological Wastewater Treatment and Resources Recovery: Attached and Suspended Growth Systems. *Water Sci. Technol.* **2019**, *80*, 2013−2026.
(25) Rodriguez-Narvaez, O. M.; Peralta-Hernandez, J. M.; Goonetilleke, A.; Bandala, E. R. Treatment Technologies for Emerging Contaminants in Water: A Review. *Chem. Eng. J.* **2017**, *323*, 361−380.
(26) Soni, R.; Bhardwaj, S.; Shukla, D. P. Various Water-Treatment Technologies for Inorganic Contaminants: Current Status and Future Aspects. *Inorg. Pollut. Water* **2020**, 273−295.
(27) Bernal, V.; Giraldo, L.; Moreno-Piraján, J. C. Adsorption of Pharmaceutical Aromatic Pollutants on Heat-Treated Activated Carbons: Effect of Carbonaceous Structure and the Adsorbent−Adsorbate Interactions. *ACS Omega* **2020**, *5*, 15247−15256.
(28) Tomczyk, A.; Sokołowska, Z.; Boguta, P. Biochar Physicochemical Properties: Pyrolysis Temperature and Feedstock Kind Effects. *Rev. Environ. Sci. Biotechnol.* **2020**, *19*, 191−215.
(29) Tsamo, C.; Assabe, M.; Argue, J.; Ihimbru, S. O. Discoloration of Methylene Blue and Slaughter House Wastewater Using Maize Cob Biochar Produced Using a Constructed Burning Chamber: A Comparative Study. *Sci. African* **2019**, *3*, No. e00078.
(30) Shamsollahi, Z.; Partovinia, A. Recent Advances on Pollutants Removal by Rice Husk as a Bio-Based Adsorbent: A Critical Review. *J. Environ. Manage.* **2019**, *246*, 314−323.
(31) Vyavahare, G.; Jadhav, P.; Jadhav, J.; Patil, R.; Aware, C.; Patil, D.; Gophane, A.; Yang, Y. H.; Gurav, R. Strategies for Crystal Violet Dye Sorption on Biochar Derived from Mango Leaves and Evaluation of Residual Dye Toxicity. *J. Cleaner Prod.* **2019**, *207*, 296−305.
(32) Law, X. N.; Cheah, W. Y.; Chew, K. W.; Ibrahim, M. F.; Park, Y. K.; Ho, S. H.; Show, P. L. Microalgal-Based Biochar in Wastewater Remediation: Its Synthesis, Characterization and Applications. *Environ. Res.* **2022**, *204*, No. 111966.
(33) Diaz-Uribe, C.; Angulo, B.; Patiño, K.; Hernández, V.; Vallejo, W.; Gallego-Cartagena, E.; Bohórquez, A. R. R.; Zarate, X.; Schott, E. Cyanobacterial Biomass as a Potential Biosorbent for the Removal of Recalcitrant Dyes from Water. *Water* **2021**, *13*, No. 3176.
(34) Ramírez-García, R.; Gohil, N.; Singh, V.Recent Advances, Challenges, and Opportunities in Bioremediation of Hazardous Materials. In *Phytomanagement of Polluted SitesMarket Opportunities in Sustainable Phytoremediation*; Elsevier, 2018; Chapter 21, pp 517−568, DOI: 10.1016/B978-0-12-813912-7.00021-1.
(35) Del Carmen, J. M. J.; Diegoalonso, R.; Diafanor, A. C.Preparation and Determination of the Functional Properties of the Trupillo Proteic Concentrated (*Prosopis Juliflora*) Preparação e Determinação Das Propriedades Funcionais Nos Concentrados de Proteínas de Trupillo*Rev.Bio.Agro*21, pp 144−152.
(36) Muller, G. C.; Junnila, A.; Traore, M. M.; Traore, S. F.; Doumbia, S.; Sissoko, F.; Dembele, S. M.; Schlein, Y.; Arheart, K. L.; Revay, E. E.; Kravchenko, V. D.; Witt, A.; Beier, J. C. The Invasive Shrub *Prosopis Juliflora* Enhances the Malaria Parasite Transmission Capacity of Anopheles Mosquitoes: A Habitat Manipulation Experiment. *Malar. J.* **2017**, *16*, No. 237.
(37) Lee, M. E.; Park, J. H.; Chung, J. W. Comparison of the Lead and Copper Adsorption Capacities of Plant Source Materials and Their Biochars. *J. Environ. Manage.* **2019**, *236*, 118−124.
(38) Vo, A. T.; Nguyen, V. P.; Ouakouak, A.; Nieva, A.; Doma, B. T.; Tran, H. N.; Chao, H. P. Efficient Removal of Cr(VI) from Water by Biochar and Activated Carbon Prepared through Hydrothermal Carbonization and Pyrolysis: Adsorption-Coupled Reduction Mechanism. *Water* **2019**, *11*, No. 1164.
(39) Lewandowski, W. M.; Januszewicz, K.; Kosakowski, W. Efficiency and Proportions of Waste Tyre Pyrolysis Products Depending on the Reactor Type-A Review. *J. Anal. Appl. Pyrolysis* **2019**, *140*, 25−53.
(40) Kwak, J. H.; Islam, M. S.; Wang, S.; Messele, S. A.; Naeth, M. A.; El-Din, M. G.; Chang, S. X. Biochar Properties and Lead(II) Adsorption Capacity Depend on Feedstock Type, Pyrolysis Temperature, and Steam Activation. *Chemosphere* **2019**, *231*, 393−404.
(41) Albalasmeh, A.; Gharaibeh, M. A.; Mohawesh, O.; Alajlouni, M.; Quzaih, M.; Masad, M.; El Hanandeh, A. Characterization and Artificial Neural Networks Modelling of Methylene Blue Adsorption of Biochar Derived from Agricultural Residues: Effect of Biomass Type, Pyrolysis Temperature, Particle Size. *J. Saudi Chem. Soc.* **2020**, *24*, 811−823.
(42) Al-Ghouti, M. A.; Da'ana, D. A. Guidelines for the Use and Interpretation of Adsorption Isotherm Models: A Review. *J. Hazard. Mater.* **2020**, *393*, No. 122383.
(43) Ayawei, N.; Ebelegi, A. N.; Wankasi, D. Modelling and Interpretation of Adsorption Isotherms. *J. Chem.* **2017**, *2017*, No. 3039817.
(44) Benjelloun, M.; Miyah, Y.; Akdemir Evrendilek, G.; Zerrouq, F.; Lairini, S. Recent Advances in Adsorption Kinetic Models: Their Application to Dye Types. *Arabian J. Chem.* **2021**, *14*, No. 103031.
(45) Kayalvizhi, K.; Alhaji, N. M. I.; Saravanakkumar, D.; Mohamed, S. B.; Kaviyarasu, K.; Ayeshamariam, A.; Al-Mohaimeed, A. M.; AbdelGawwad, M. R.; Elshikh, M. S. Adsorption of Copper and Nickel by Using Sawdust Chitosan Nanocomposite Beads − A Kinetic and Thermodynamic Study. *Environ. Res.* **2022**, *203*, No. 111814.
(46) Qin, L.; Wu, Y.; Hou, Z.; Jiang, E. Influence of Biomass Components, Temperature and Pressure on the Pyrolysis Behavior and Biochar Properties of Pine Nut Shells. *Bioresour. Technol.* **2020**, *313*, No. 123682.
(47) Valencia, L.; Arumughan, V.; Jalvo, B.; Maria, H. J.; Thomas, S.; Mathew, A. P. Nanolignocellulose Extracted from Environmentally Undesired *Prosopis Juliflora*. *ACS Omega* **2019**, *4*, 4330−4338.
(48) Mian, M. M.; Liu, G. Recent Progress in Biochar-Supported Photocatalysts: Synthesis, Role of Biochar, and Applications. *RSC Adv.* **2018**, *8*, 14237−14248.
(49) Liu, D.; Zhang, W.; Lin, H.; Li, Y.; Lu, H.; Wang, Y. A Green Technology for the Preparation of High Capacitance Rice Husk-Based Activated Carbon. *J. Cleaner Prod.* **2016**, *112*, 1190−1198.
(50) Sotoudehnia, F.; Baba Rabiu, A.; Alayat, A.; McDonald, A. G. Characterization of Bio-Oil and Biochar from Pyrolysis of Waste Corrugated Cardboard. *J. Anal. Appl. Pyrolysis* **2020**, *145*, No. 104722.
(51) Lu, X.; Qiu, W.; Ma, J.; Xu, H.; Wang, D.; Cheng, H.; Zhang, W.; He, X. The Overestimated Role of Singlet Oxygen for Pollutants Degradation in Some Non-Photochemical Systems. *Chem. Eng. J.* **2020**, *401*, No. 126128.
(52) Ghodake, G. S.; Shinde, S. K.; Kadam, A. A.; Saratale, R. G.; Saratale, G. D.; Kumar, M.; Palem, R. R.; AL-Shwaiman, H. A.; Elgorban, A. M.; Syed, A.; Kim, D. Y. Review on Biomass Feedstocks, Pyrolysis Mechanism and Physicochemical Properties of Biochar: State-of-the-Art Framework to Speed up Vision of Circular Bioeconomy. *J. Cleaner Prod.* **2021**, *297*, No. 126645.

https://doi.org/10.1021/acsomega.2c05007
ACS Omega 2022, 7, 42916−42925

(53) Gupta, S.; Kawale, H. D.; Ahmed, G.; Acharya, S.; Kishore, N. Effect of Temperature on Catalytic Pyrolysis of Polyalthia Longifolia Leaves Solid Waste and Characterization of Their Products. *Curr. Res. Green Sustainable Chem.* **2021**, *4*, No. 100062.
(54) Jin, Y.; Zhang, M.; Jin, Z.; Wang, G.; Li, R.; Zhang, X.; Liu, X.; Qu, J.; Wang, H. Characterization of Biochars Derived from Various Spent Mushroom Substrates and Evaluation of Their Adsorption Performance of Cu(II) Ions from Aqueous Solution. *Environ. Res.* **2021**, *196*, No. 110323.
(55) Suciu, L. G.; Masiello, C. A.; Griffin, R. J. Anhydrosugars as Tracers in the Earth System. *Biogeochemistry* **2019**, *146*, 209−256.
(56) Das, O.; Mensah, R. A.; George, G.; Jiang, L.; Xu, Q.; Neisiany, R. E.; Umeki, K.; Jose E, T.; Phounglamcheik, A.; Hedenqvist, M. S.; Restás, Á.; Sas, G.; Försth, M.; Berto, F. Flammability and Mechanical Properties of Biochars Made in Different Pyrolysis Reactors. *Biomass Bioenergy* **2021**, *152*, No. 106197.
(57) Sahoo, S. S.; Vijay, V. K.; Chandra, R.; Kumar, H. Production and Characterization of Biochar Produced from Slow Pyrolysis of Pigeon Pea Stalk and Bamboo. *Cleaner Eng. Technol.* **2021**, *3*, No. 100101.
(58) Subratti, A.; Vidal, J. L.; Lalgee, L. J.; Kerton, F. M.; Jalsa, N. K. Preparation and Characterization of Biochar Derived from the Fruit Seed of Cedrela Odorata L and Evaluation of Its Adsorption Capacity with Methylene Blue. *Sustainable Chem. Pharm.* **2021**, *21*, No. 100421.
(59) Lam, Y. Y.; Lau, S. S. S.; Wong, J. W. C. Removal of Cd(II) from Aqueous Solutions Using Plant-Derived Biochar: Kinetics, Isotherm and Characterization. *Bioresour. Technol. Rep.* **2019**, *8*, No. 100323.
(60) Ahmad, M.; Rajapaksha, A. U.; Lim, J. E.; Zhang, M.; Bolan, N.; Mohan, D.; Vithanage, M.; Lee, S. S.; Ok, Y. S. Biochar as a Sorbent for Contaminant Management in Soil and Water: A Review. *Chemosphere* **2014**, *99*, 19−33.
(61) Calzaferri, G.; Gallagher, S. H.; Brühwiler, D. Multiple Equilibria Describe the Complete Adsorption Isotherms of Non-porous, Microporous, and Mesoporous Adsorbents. *Microporous Mesoporous Mater.* **2022**, *330*, No. 111563.
(62) Shen, L.; Zhang, L.; Wang, K.; Miao, L.; Lan, Q.; Jiang, K.; Lu, H.; Li, M.; Li, Y.; Shen, B.; Zheng, W. Analysis of Oxidation Degree of Graphite Oxide and Chemical Structure of Corresponding Reduced Graphite Oxide by Selecting Different-Sized Original Graphite. *RSC Adv.* **2018**, *8*, 17209−17217.
(63) Mukome, F. N.; Parikh, S. J.Chemical, Physical, and Surface Characterization of Biochar. In *Biochar: Production, Characterization, and Applications*; CRC Press: New York, 2015; pp 67−91.
(64) Guo, Y.; Zhang, H.; Liu, Y. Desorption Characteristics and Kinetic Parameters Determination of Molecular Sieve by Thermogravimetric Analysis/Differential Thermogravimetric Analysis Technique. *Adsorpt. Sci. Technol.* **2018**, *36*, 1389−1404.
(65) Xu, Q.; Tang, S.; Wang, J.; Ko, J. H. Pyrolysis Kinetics of Sewage Sludge and Its Biochar Characteristics. *Process Saf. Environ. Prot.* **2018**, *115*, 49−56.
(66) Gao, L.; Li, Z.; Yi, W.; Li, Y.; Zhang, P.; Zhang, A.; Wang, L. Impacts of Pyrolysis Temperature on Lead Adsorption by Cotton Stalk-Derived Biochar and Related Mechanisms. *J. Environ. Chem. Eng.* **2021**, *9*, No. 105602.
(67) Pawar, A.; Panwar, N. L. A Comparative Study on Morphology, Composition, Kinetics, Thermal Behaviour and Thermodynamic Parameters of *Prosopis Juliflora* and Its Biochar Derived from Vacuum Pyrolysis. *Bioresour. Technol. Rep.* **2022**, *18*, No. 101053.
(68) Stylianou, M.; Christou, A.; Dalias, P.; Polycarpou, P.; Michael, C.; Agapiou, A.; Papanastasiou, P.; Fatta-Kassinos, D. Physicochemical and Structural Characterization of Biochar Derived from the Pyrolysis of Biosolids, Cattle Manure and Spent Coffee Grounds. *J. Energy Inst.* **2020**, *93*, 2063−2073.
(69) Hung, C. Y.; Tsai, W. T.; Chen, J. W.; Lin, Y. Q.; Chang, Y. M. Characterization of Biochar Prepared from Biogas Digestate. *Waste Manage.* **2017**, *66*, 53−60.
(70) Bardalai, M.; Mahanta, D. K. Characterisation of Biochar Produced by Pyrolysis from Areca Catechu Dust. *Mater. Today Proc.* **2018**, *5*, 2089−2097.
(71) Heitkötter, J.; Marschner, B. Interactive Effects of Biochar Ageing in Soils Related to Feedstock, Pyrolysis Temperature, and Historic Charcoal Production. *Geoderma* **2015**, *245*−*246*, 56−64.
(72) Selvarajoo, A.; Oochit, D. Effect of Pyrolysis Temperature on Product Yields of Palm Fibre and Its Biochar Characteristics. *Mater. Sci. Energy Technol.* **2020**, *3*, 575−583.
(73) Saravanan, A.; Sundararaman, T. R.; Jeevanantham, S.; Karishma, S.; Kumar, P. S.; Yaashikaa, P. R. Effective Adsorption of Cu(II) Ions on Sustainable Adsorbent Derived from Mixed Biomass (Aspergillus Campestris and Agro Waste): Optimization, Isotherm and Kinetics Study. *Groundwater Sustainable Dev.* **2020**, *11*, No. 100460.
(74) Wang, Y.; Zhang, Y.; Li, S.; Zhong, W.; Wei, W. Enhanced Methylene Blue Adsorption onto Activated Reed-Derived Biochar by Tannic Acid. *J. Mol. Liq.* **2018**, *268*, 658−666.
(75) Húmpola, P. D.; Odetti, H. S.; Fertitta, A. E.; Vicente, J. L. Thermodynamic Analysis of Adsorption Models of Phenol in Liquid Phase on Different Activated Carbons. *J. Chil. Chem. Soc.* **2013**, *58*, 1541−1544.
(76) Xu, D.; Cao, J.; Li, Y.; Howard, A.; Yu, K. Effect of Pyrolysis Temperature on Characteristics of Biochars Derived from Different Feedstocks: A Case Study on Ammonium Adsorption Capacity. *Waste Manage.* **2019**, *87*, 652−660.
(77) Hu, X.; Zhang, X.; Ngo, H. H.; Guo, W.; Wen, H.; Li, C.; Zhang, Y.; Ma, C. Comparison Study on the Ammonium Adsorption of the Biochars Derived from Different Kinds of Fruit Peel. *Sci. Total Environ.* **2020**, *707*, No. 135544.
(78) Sewu, D. D.; Boakye, P.; Woo, S. H. Highly Efficient Adsorption of Cationic Dye by Biochar Produced with Korean Cabbage Waste. *Bioresour. Technol.* **2017**, *224*, 206−213.
(79) Santoso, E.; Ediati, R.; Kusumawati, Y.; Bahruji, H.; Sulistiono, D. O.; Prasetyoko, D. Review on Recent Advances of Carbon Based Adsorbent for Methylene Blue Removal from Waste Water. *Mater. Today Chem.* **2020**, *16*, No. 100233.
(80) Bedin, K. C.; Martins, A. C.; Cazetta, A. L.; Pezoti, O.; Almeida, V. C. KOH-Activated Carbon Prepared from Sucrose Spherical Carbon: Adsorption Equilibrium, Kinetic and Thermodynamic Studies for Methylene Blue Removal. *Chem. Eng. J.* **2016**, *286*, 476−484.
(81) Alalwan, H. A.; Mohammed, M. M.; Sultan, A. J.; Abbas, M. N.; Ibrahim, T. A.; Aljaafari, H. A. S.; Alminshid, A. A. Adsorption of Methyl Green Stain from Aqueous Solutions Using Non-Conventional Adsorbent Media: Isothermal Kinetic and Thermodynamic Studies. *Bioresour. Technol. Rep.* **2021**, *14*, No. 100680.
(82) Peydayesh, M.; Rahbar-Kelishami, A. Adsorption of Methylene Blue onto Platanus Orientalis Leaf Powder: Kinetic, Equilibrium and Thermodynamic Studies. *J. Ind. Eng. Chem.* **2015**, *21*, 1014−1019.
(83) Kumar, M.; Tamilarasan, R. Modeling Studies for the Removal of Methylene Blue from Aqueous Solution Using Acacia Fumosa Seed Shell Activated Carbon. *J. Environ. Chem. Eng.* **2013**, *1*, 1108−1116.
(84) Islam, M. A.; Sabar, S.; Benhouria, A.; Khanday, W. A.; Asif, M.; Hameed, B. H. Nanoporous Activated Carbon Prepared from Karanj (*Pongamia pinnata*) Fruit Hulls for Methylene Blue Adsorption. *J. Taiwan Inst. Chem. Eng.* **2017**, *74*, 96−104.
(85) Sahu, S.; Pahi, S.; Tripathy, S.; Singh, S. K.; Behera, A.; Sahu, U. K.; Patel, R. K. Adsorption of Methylene Blue on Chemically Modified Lychee Seed Biochar: Dynamic, Equilibrium, and Thermodynamic Study. *J. Mol. Liq.* **2020**, *315*, No. 113743.
(86) Ahmad Khan, F.; Farooqui, M. Removal of Methylene Blue Dye from Aqueous Solutions onto *Morus Nigra* L. (Mulberry Tree) Leaves Powder and Its Biochar- Equilibrium, Kinetic and Thermodynamic Study. *Int. J. Environ. Anal. Chem.* **2022**, 1−20.

https://doi.org/10.1021/acsomega.2c05007
ACS Omega 2022, 7, 42916−42925